JOURNAL OF GEOPHYSICAL RESEARCH, VOL. 106, NO. A1, PAGES 107–116, JANUARY 1, 2001

Auroral particle transport using Monte Carlo and hybrid methods

Stanley C. Solomon

Laboratory for Atmospheric and Space Physics, University of Colorado, Boulder

Abstract. A numerical model of energetic electron transport in the thermosphere and middle atmosphere has been extended for application to proton aurora. The electron model employs a Monte Carlo method for the primary flux and either a full Monte Carlo or two-stream method for secondary electrons. The hybrid Monte Carlo / two-stream (MC2S) method has been adapted to the case of auroral proton / hydrogen atom / secondary electron fluxes. The methodology for implementation of these models is described, and selected results are compared to other algorithms. Good agreement is obtained with recent results using equation of transfer methods.

1. Introduction

The transport of energetic auroral electrons and protons in the upper atmosphere is an engaging subdivision of the field of radiative transfer. Numerical techniques for calculating fluxes, ionization rates, and other forms of energy deposition by electrons, protons, and other charged and neutral particles have been developed by several investigators. The electron transport methods are the most highly developed and intensively used, since the majority of auroral phenomena are caused by energetic electrons. However, advances in auroral proton / hydrogen atom modeling have occurred as well. Recent work on H^+/H aurora is reviewed by *Galand et al.* [1997] and *Galand* [this issue].

The energy distribution of primary auroral particles determines the altitude z_{max} at which peak ionization occurs. This energy distribution is often specified by a single parameter, the "characteristic energy" E_0, referring to, for instance, the peak of an assumed Maxwellian energy distribution. Estimation of E_0 by spectroscopic means enables remote approximation of z_{max}, which is an important quantity for ionospheric conductance and hence for general circulation models of the thermosphere. Accurate models are necessary to accomplish this. Auroral particle transport poses particular numerical challenges, primarily because of the difficulty of performing energy redistribution calculations on energies that can range over 9 orders of magnitude. The most intense, and lowest altitude, auroral phenomena are generally caused by the highest energy particles in a distribution entering the atmosphere (the primary flux), but much of the excitation and molecular dissociation is dominated by the low energy electrons that result from energy cascade and secondary electron generation processes. Details of distribution functions, cross sections, and numerical implementations can lead to varying results.

We may divide the many types of approaches to auroral particle transport modeling into three broad categories: continuous loss methods, equation of transfer methods, and Monte Carlo methods. Continuous loss methods implement laboratory results or other estimates of the aggregate effect of a particle beam interacting with matter, and obtain an appropriate fit function on a spatial grid. Equation of transfer methods attempt to solve the Boltzmann equation by discretizing the energy, angular, and spatial dimensions and integrating the collisional redistribution of particles in this space. Monte Carlo methods discretize the individual particles instead.

Continuous loss methods are the most direct way to perform auroral transport calculations, but equation of transfer methods are more powerful and elegant. In moving from the atomic scale (cross sections, etc.) to the atmospheric scale (altitude distribution of ionization rates, etc.), there is always the question of whether the model predictions are valid, particularly when there are discrepancies between results from an equation of transfer method and continuous loss results that are essentially direct renormalizations of laboratory measurements. Because the extensive energy range necessitates variably spaced energy grid intervals and requires special techniques for computation of the redistribution function, problems with numerical algorithms can be difficult to evaluate and resolve.

In this context a natural choice is the Monte Carlo approach, which avoids the energy grid problem altogether. This method has been applied to electron transport, [e.g., *Berger et al.*, 1970, 1974; *Cicerone and Bowhill*, 1971], but Berger et al. did not perform secondary electron flux calculations, and Cicerone and Bowhill examined the photoelectron case, which, owing to the smaller range of energies, is much easier to solve. *Porter and Green* [1975] have also applied the Monte Carlo method to low-energy auroral proton transport. Work by *Onda et al.* [1992], *Kozelov and Ivanov* [1992, 1994], *Kozelov* [1993], and *Synnes et al.* [1998], employing Monte Carlo methods for aspects of electron and proton transport, have renewed interest in this subject. *Solomon* [1993] presented initial results from Monte Carlo calculations of electron transport. *Gattinger et al.* [1996] implemented a similar auroral electron model.

The original motivation for constructing a Monte Carlo model [*Solomon*, 1993] was to address the issue of whether emissions excited in aurora by low-energy secondary electrons vary as a function of characteristic energy of the primary flux. Calculations by *Lummerzheim et al.* [1989] and *Rees and Lummerzheim* [1989] showed a large dependence, contradicting the results of *Strickland et al.* [1976, 1989], who found negligible dependence for $E_0 > \sim 1$ keV. *Solomon* [1993] concluded that the dependence was indeed negligible, and subsequent revisions by *Lummerzheim and Lilensten* [1994] agreed. However, for proton / hydrogen atom aurora the secondary electron distribution can be a function of primary particle energy, so these conclusions do not apply.

Monte Carlo methods are thought of as brute force: they are time consuming and in some sense less elegant than equation of transfer solutions. However, they integrate in the way that nature

Paper number 2000JA002011.
0148-0227/01/2000JA002011$09.00

does, and at some level they are the most realistic simulations possible. This does not mean that the mathematics are necessarily simplified, or that approximations are entirely avoided. A great deal of effort for Monte Carlo techniques goes into the attempt to find analytic, integrable fit functions that describe fundamental distributions such as scattering phase angle and secondary electron energy. The basic technique is then to take the indefinite integral of the fit function, and equate it to a uniformly distributed number obtained from a pseudorandom generation algorithm and normalized to the range of the fit function abscissa. The fitted parameter is solved for as a function of the random number. This scales the cumulative distribution of the fitted parameter to the uniform distribution of the random number, and enables rapid computation of appropriately distributed quantities. Probabilistic decisions can also be implemented by grid searches and interpolation, but this is generally less efficient.

The goal of this work is to perform auroral particle transport calculations using a complete model that addresses all aspects of the problem, including all collisional energy transfer processes, scattering processes, secondary electron generation, and their subsequent transport, for all major atmospheric species and altitudes, that is applicable to the full range of energetic particles observed in the terrestrial atmosphere. Ultimately, this will include magnetic field effects and transport in the horizontal dimensions. In this paper, results are shown for computations as a function of altitude, under the collisional regime.

2. Method

2.1. Monte Carlo Electron Model

The electron transport model operates in a spatial dimension, an angular dimension, and an energy dimension. The spatial dimension is along a magnetic field line, and the angular dimension is the pitch angle to that field line. Other than an interpolation "mesh" in energy and altitude for calculation of cross sections and densities and tabulation of results, there is no explicit gridding or binning of an electron's location in this space. The underlying assumptions are those characteristic of collisional electron transport models: that electric field acceleration, magnetic field variation, and gravity have negligible effect; that the electrons are confined to spiral paths about a magnetic field line characterizable by a pitch angle distribution; and that wave-plasma interactions are unimportant in the thermosphere.

An electron enters the upper level of a model atmosphere (~900 km) with an initial energy and pitch angle, and is subjected to a sequence of pseudorandom collision events, resulting in a new altitude, pitch angle, and energy after each. For computation of spatial transport the electrical depth τ_e is defined as the sum over all atmospheric species of the product of column density and total electron impact cross section, in analogy to the definition of optical depth:

$$\tau_e = \sum_i N_i \sigma_{\mathrm{tot}_i} \quad . \tag{1}$$

The mean free path of the electron is the distance at which $\Delta\tau_e$=1. The randomized distance that an electron will move before its next collision is determined from Beer's law, using the method described by *Meier and Lee* [1978]. If r is a number randomly distributed between 0 and 1, then

$$\Delta\tau_e = -\ln(r) \quad . \tag{2}$$

The change in altitude is then calculated, taking into account the current pitch angle and magnetic field angle. The type of collision (elastic, excitation, dissociation, or ionization) is determined randomly, weighted by products of cross sections and densities at the collision location. The species and specific state transition are also determined randomly, using cross section ratios. The primary electron energy is then reduced by an amount equal to the sum of the excitation, dissociation, and ionization energy plus the secondary electron energy, if any.

If the collision is an ionizing collision, a secondary electron is created, randomly assigned an isotropically distributed pitch angle, and randomly assigned an energy using an integral form of the formula of *Green and Sawada* [1972] and *Jackman et al.* [1977] (which is based on the laboratory results of *Opal et al.* [1971]):

$$\int_0^{E_s} \sigma_{i,j}(E_p, E_s')\,dE_s' = A(E_p)\Gamma(E_p)\left[\tan^{-1}\left(\frac{E_s - T_0(E_p)}{\Gamma(E_p)}\right) + c\right], \tag{3}$$

where $\sigma_{i,j}$ is the state-specific cross section for species i and state j at primary energy E_p and secondary energy E_s, $A(E_p)$, $\Gamma(E_p)$, and $T_0(E_p)$ are fitting functions defined by the tabulated parameters of Jackman et al., and c=tan^{-1}[$T_0(E_p)/\Gamma(E_p)$]. By equating the integral to a random number r, dropping the leading constants, and solving for E_s, randomized secondary electron generation functions distributed according to the above parameterizations are obtained:

$$E_s = \Gamma(E_p)\tan(r - c) + T_0(E_p) \quad , \tag{4}$$

where r has been normalized over the interval 0 to $r_{\max}$:

$$r_{\max} = \tan^{-1}\left[\frac{E_{s\max} - T_0(E)}{\Gamma(E)}\right] + c; \quad E_{s_{\max}} = \frac{E_p - E_{\mathrm{ion}}}{2} \quad . \tag{5}$$

If the collision is elastic, the electron is randomly given a new pitch angle using expressions and parameters developed by *Porter and Jump* [1978] and *Porter et al.* [1987] for angular scattering of electrons. This phenomenological extension to the screened Rutherford formula allows a backscattering lobe at low energy:

$$\sigma(\theta) = \alpha\left[\frac{1}{(1 + 2\gamma - \cos\theta)} + \frac{\beta}{(1 + 2\delta + \cos\theta)}\right], \tag{6}$$

where α, β, γ, and δ are fit parameters, tabulated as functions of energy. Porter and Jump also derived the cumulative distribution, which is used to produce a change of pitch angle θ:

$$\cos\theta = \frac{-A \pm \sqrt{A^2 - 4B}}{2} \quad , \tag{7}$$

$$A = 2\delta - 2\gamma + \frac{\beta + 1}{\frac{\sigma r}{2\pi\alpha} + \frac{1}{2 + 2\gamma} - \frac{\beta}{2\delta}} \quad ,$$

$$B = -(1 + 2\delta + 2\gamma + 4\delta\gamma) + \frac{1 + 2\delta - \beta(1 + 2\gamma)}{\frac{\sigma r}{2\pi\alpha} + \frac{1}{2 + 2\gamma} - \frac{\beta}{2\delta}} \quad .$$

For inelastic collisions the forward scattering approximation is made: it is assumed that the phase function from these collisions is so strongly peaked in the forward direction that angular redistribution by this means is negligible. That should be a good approximation at all but the lowest energies; below 100 eV there can be considerable backscatter, particularly from forbidden excitation transitions, but the flux becomes so isotropic and the relative size of the elastic cross sections becomes so large that this has little effect on the final pitch angle distribution.

After the collision parameters have been calculated and the electron energy and/or pitch angle has been changed, a new $\Delta\tau_e$ is obtained, and the process is continued until the primary electron exits the upper boundary or is thermalized. This is then repeated for each secondary electron created during passage of the primary, and the tertiaries created by the secondaries, and so on, until there are none left. The procedure is then recapitulated for another primary. For most purposes, 10^4–10^5 primary electrons, with a specified (e.g., Maxwellian, Gaussian, or monoenergetic) initial energy distribution and a specified (e.g., isotropic, cosine, or monodirectional) initial pitch angle distribution are used for a particular run to obtain reasonable statistics in the energy spectra; if details of the angular distribution are desired, a larger number may be necessary. Ionization, excitation, dissociation, and heating rates are obtained by accumulating event counts at each altitude level. Fluxes are tabulated by counting each altitude level crossing within each energy and pitch angle bin. The accumulations are then normalized to a specified total energy flux. Energy conservation is monitored and maintained to approximately one part in 10^6.

Cross sections for elastic collisions, dissociation, and state-specific excitation and ionization are obtained from a variety of laboratory and theoretical sources. The approach used by *Solomon et al.* [1988] is adopted here. That method is to interpolate from tabulated values for elastic cross sections but to employ analytic fit functions for inelastic cross sections, using the *Green and Sawada* [1972] and *Jackman et al.* [1977] formula for ionization and the *Green and Stolarski* [1972] equation for excitation. The Jackman et al. cross section parameters were retained, with the exception of the linear coefficients for O which were adjusted to match the results of *Burnett and Rountree* [1979] as suggested by *Link* [1982]. The Green and Stolarski cross sections were re-fit to more recent laboratory data as described by Solomon et al. There have been minor revisions to the cross sections used in that work for the triplet and quintet systems of atomic oxygen, incorporating measurements of *Gulcicek and Doering* [1988], *Gulcicek et al.* [1988], and *Doering and Gulcicek* [1989]. Heating of the ambient (thermal) electron gas and the consequent degradation of energetic electrons are calculated using *Swartz et al.'s* [1971] relationship.

2.2. Monte Carlo / Two-Stream Hybrid Electron Model

At low energy, elastic cross sections become so much larger than inelastic cross sections that an electron makes repeated collisions without losing significant energy. Transport is generally negligible in this regime, except at the highest altitudes, so the way this is dealt with in the Monte Carlo code is that below 2 eV, local energy deposition is assumed. However, a disproportionate amount of computational time is spent on low-energy electrons in the 2–10 eV range, which seldom move far from their source before being thermalized. In fact, secondary electron transport is negligible below ~200 km, and the distribution is nearly isotropic throughout the thermosphere. In the exosphere we wish to maintain the ability to model non-isotropic fluxes so that the escaping upward flux (or "backscattered," although most of it is generated internal to the thermosphere) may be calculated. For these reasons, neglecting the transport of secondary electrons is not advisable, but a detailed calculation of pitch angle distributions is not necessary. The situation for auroral secondary electrons is analogous to the photoelectron case, where a two-stream approximation to the electron flux is valid. The two-stream approximation may also be used for primary auroral fluxes, although not for highly anisotropic pitch angle distributions.

To exploit this difference between requirements for primary and secondary transport calculations, a "hybrid" approach is adopted. The method uses the Monte Carlo algorithm described above, but rather than recursively feeding the secondary electrons back into the code, secondary production is tabulated for each altitude and energy bin. Then, after the Monte Carlo run is complete, this secondary production function is input to a two-stream model in a manner completely analogous to the way that photoelectron production would be handled. The model employed for secondaries is described by *Solomon et al.* [1988] and *Solomon and Abreu* [1989] and is based on the original two-stream algorithm of *Banks and Nagy* [1970] and *Banks et al.* [1974]. It is a member of the class of equation of transfer methods but uses the simplification that the pitch angle distribution may be approximated by discretization into two categories, upward and downward, with an average or characteristic pitch angle cosine (here ± 0.5) describing each. Hemispherically integrated fluxes as a function of energy, and ionization, excitation, dissociation, and heating rates as a function of altitude, are then combined from the two model outputs.

The Monte Carlo / two-stream model (henceforth "MC2S") is found to be adequate for auroral calculations. The MC2S model has been compared to the "pure" Monte Carlo for a variety of cases, as briefly described in the section 3.1. The differences are small, and negligible for quantities that integrate over an energy range, such as ionization or excitation rates. The benefit in computational efficiency of using the MC2S method is dramatic, up to two orders of magnitude, a few minutes instead of a few hours on a typical *fin-de-siècle* desktop computer.

2.3. Extension to Relativistic Energies

Calculations for high-energy particles take proportionally longer than those for auroral energies do because there are more collisions per input particle, yet it still takes at least 10^4 particles to build up acceptable statistics. With the MC2S method these computations may nevertheless be performed in reasonable times, although not as efficiently as with the two-stream algorithm. These models have therefore been extended to high energy to enable calculation of high energy electrons, including, in principle, highly relativistic energies out to 1 GeV.

The key factors in this extension are the ionization cross sections and secondary electron production functions. Elastic collisions become so strongly peaked in the forward direction at high energies that their effect becomes negligible, and excitation cross sections become proportionally less important than ionization. The total ionization cross sections for N_2 calculated by *Porter et al.* [1976] are in accord with measurements (up to 2.7 MeV) by *Rieke and Prepejchal* [1972] and with recent theoretical analysis [*Saksena et al.*, 1997] and so are adopted here. These results show the same behavior at high energy for O_2. The implementation here is simply to calculate the ratio of the Porter et al. relativistic cross section to the *Jackman et al.* [1977] non-relativistic cross section for ionization of N_2 as a function of energy, and to apply that ratio to all three major species (N_2, O_2, and O). Interestingly, the cross sections start to increase at 1 MeV. However, they do not increase as fast as the energy of the electrons, so the "stopping power" of atmospheric gases continues to decline as it takes more collisions to thermalize a higher energy electron: higher energy electrons still penetrate deeper into the atmosphere.

There is little information available on the distribution of secondary electrons generated by relativistic primaries. The *Opal et al.* [1971] measurements show no significant change of production spectrum shape with primary energy above ~1 keV, so the

Jackman et al. [1977] fit to these data is used at high energy as well. Secondary production has little effect on peak altitude and ionization rates, but it can be important for excitation rates of transitions that peak at low energy and hence for spectroscopic analysis.

2.4. Proton Model

Modeling particle transport in proton aurora presents particular difficulties, because the phenomenon couples fluxes of protons, hydrogen atoms, and electrons. Fortunately, the electron flux does not significantly affect the proton / hydrogen atom flux in the collisional regime, so the generation and transport of secondary electrons may be handled using either of the techniques described in sections 2.1 and 2.2 for electron aurora. The choice was made to proceed with the MC2S approach, since it has been satisfactory for electron calculations. Proton and hydrogen atom fluxes are computed using the Monte Carlo method, and secondary electron fluxes generated thereby are calculated using the two-stream method.

Application of the method described in section 2.1 to protons proceeds in an analogous fashion, but with the critical difference that the collision types and cross sections change as the particle changes from a proton to a hydrogen atom and back through the processes of charge exchange and electron stripping. The algorithm follows an individual particle and changes an index marking its charge state, applying the appropriate collision parameters in either case. Energy is lost in each of these collisions, but rather than using an average energy loss approximation for each collision type [e.g., *Basu et al.*, 1993], the energy loss for each collision is explicitly calculated, depending on the energy of the individual secondary electron generated (if any). However, unlike the electron algorithm, total excitation and ionization cross sections are used for each species rather than individual states, since there is much less information available for individual state transitions due to proton and hydrogen atom impact. This necessitates the assumption of an average excitation energy and an average ionization potential (including dissociated and excited ion states); following Basu et al. we adopt 17, 15, and 16 eV for ionization, and 10, 8, and 12 eV for excitation of N_2, O_2, and O, respectively.

To guide our thinking for energy loss and ion or electron generation in the four types of collisions, Table 1 is presented. E_i and I_i are the average excitation energy and ionization potential for species i, I_H is the average ionization potential for hydrogen (~13.6 eV), and S is the energy of the secondary electron generated by the collision. The cross sections adopted for these processes are taken from the survey by *Basu et al.* [1987].

A critical matter in proton auroral modeling is the energy distribution of secondary electron production. Laboratory measurements by *Crooks and Rudd* [1971] and *Toburen* [1971] for protons in the 50 keV to 1 MeV range on N_2 were analyzed by *Porter et al.* [1976], showing a shape similar to that generated for electrons using the *Jackman et al.* [1977] formula discussed in section 2.1, including a power law decay at energy > ~20 eV and little or no dependence of the shape on primary energy above 100 keV. However, subsequent work using protons at 5–70 keV [*Rudd*, 1979, 1988] showed an exponential decay, with significant dependence of the logarithmic slope on primary energy, as discussed by *Basu et al.* [1993]. For this work a simple exponential function is adopted, hence the secondary electron component of this model must be used with caution above 100 keV. The Rudd $H^+ + N_2$ measurements are fit with a function of the form

$$\sigma_i(E_s) = \exp(-\alpha E_s)\,, \tag{8}$$

where E_s is the secondary electron energy and α is a function of primary proton energy with the empirically derived form

$$\alpha(E_p) = 0.034 \ln\left[\frac{1.8\times10^5}{E_p}\right]. \tag{9}$$

The same secondary electron energy distribution parameters are assumed for O_2 and O, although different ionization cross sections are used. This results in a secondary electron energy distribution that is considerably lower in average energy than corresponding distributions from primary electrons, and becomes more so at lower (<20 keV) proton energies. Following Porter et al. and Basu et al., and in the absence of evidence to the contrary, the same distribution is assumed for secondary electrons generated by hydrogen atom impact ionization.

In order to generate a randomized secondary electron distribution, the integral form must be employed:

$$\int \sigma(E_s)dE_s = -\frac{1}{\alpha}\exp(-\alpha E_s) + c = \frac{1-\exp(-\alpha E_s)}{\alpha} = r\,, \tag{10}$$

$$E_s = \frac{-\ln(1-\alpha r)}{\alpha}\,, \tag{11}$$

where r is a pseudorandom number distributed over the interval 0 to $r_{max}=1/\alpha$.

For ionization collisions, isotropically distributed secondaries are generated using this method. For electron stripping, the assumption is made, following *Basu et al.* [1993], that the secondary distribution function is the same with respect to energy and direction, but in the rest frame of the energetic hydrogen atom. When transformed back into the atmospheric rest frame, this results in a higher energy distribution that favors the direction of motion of the hydrogen atom; this effect becomes particularly significant at high energy. To perform this transform, the initial velocity $v_0=(2E_H/m_H)^{1/2}$ and secondary velocity in the hydrogen atom rest frame $v_1=(2E_e/m_e)^{1/2}$ are calculated from the hydrogen atom energy E_H and mass m_H and the secondary electron energy E_e and mass m_e, respectively. Then, using the law of cosines:

$$\begin{aligned} v_s &= \left(v_0^2 + v_1^2 - 2\mu_1 v_0 v_1\right)^{1/2} \\ E_s &= \frac{m_e v_s^2}{2} \\ \Delta\mu_s &= \frac{v_0 - \mu_1 v_1}{v_s} \end{aligned} \tag{12}$$

where μ_1 is the secondary electron pitch angle cosine in the hydrogen atom rest frame, v_s and E_s are the velocity and energy of

Table 1. Energy Loss in H+ and H Collisions

Collision Type	Ion Generated?	Secondary Electron?	Energy Loss
Excitation: $(H^+ \text{ or } H)+M \rightarrow M^*$	–	–	E_i
Ionization: $(H^+ \text{ or } H)+M \rightarrow M^+$	✓	✓	$I_i + S$
Charge Exchange: $H^+ + M \rightarrow H + M^+$	✓	–	$I_i - I_H$
Electron Stripping: $H+M \rightarrow H^+ + M + e^*$	–	✓	$I_H + S$

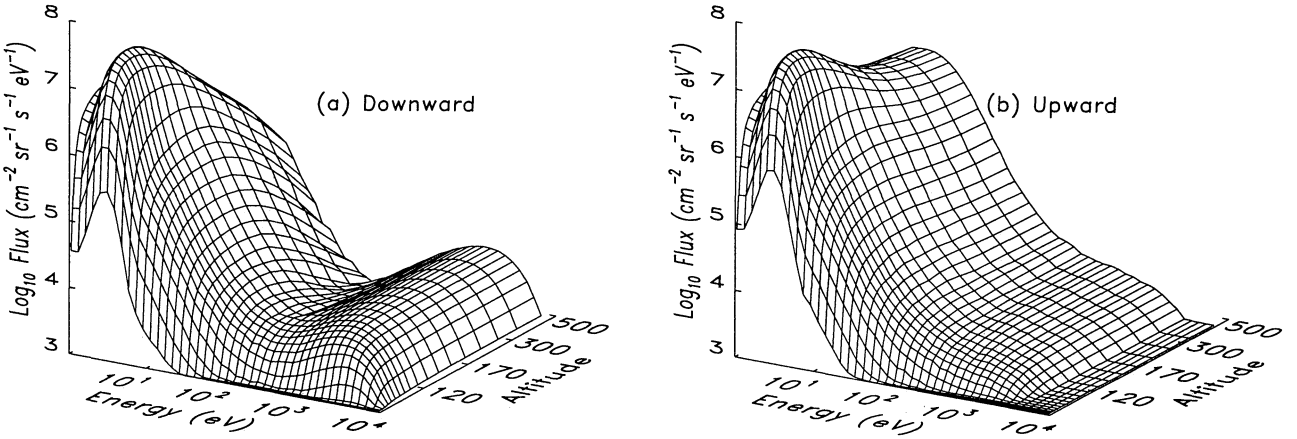

Figure 1. Model electron fluxes as a function of altitude and energy. A Maxwellian flux, total energy Q_0=1 erg cm^{-2} s^{-1}, characteristic energy E_0=2 keV, isotropic over the downward hemisphere, was input to the "top" of the atmosphere at 900 km. (a) Flux averaged over the downward hemisphere. (b) Flux averaged over the upward hemisphere.

the secondary electron in the atmosphere, and $\Delta\mu_s$ is the amount by which the pitch angle cosine is changed from the primary pitch angle.

As with the electron model, the forward scattering approximation is made for inelastic collisions. In addition, with little certainty on the cross sections or phase functions of elastic scattering of protons and hydrogen atoms, other than that they are extremely forward-peaked for the energies evaluated here, elastic pitch angle distribution is neglected as well. This assumption is the same as that made for comparative work shown in section 4.2, so it is at least a consistent basis for comparison.

3. Results

3.1. Electrons

A variety of auroral conditions have been tested; a limited selection of results are presented here. Figure 1 is a plot of calculated electron flux as a function of altitude and energy. A Maxwellian energy distribution, characteristic energy E_0=2 keV, total energy flux Q_0=1 erg cm^{-2} s^{-1}, isotropically distributed in pitch angle over the downward hemisphere, was applied to the "top" of the atmosphere at 900 km. The 1986 Mass Spectrometer Incoherent Scatter (MSIS-86) model atmosphere for moderate solar activity, $F_{10.7}$=<$F_{10.7}$>=150, A_p=30, was employed [*Hedin*, 1987]. A total of 5×10^4 primary electrons were used to create the Maxwellian distribution, which is equivalent to a 200 MeV energy flux. The results were then normalized to a 1 erg cm^{-2} s^{-1} flux. Fluxes averaged over the downward traveling hemisphere and upward traveling hemisphere are shown in Figures 1a and 1b, respectively.

Total ionization rate profiles calculated as a function of altitude are shown in Figure 2. All input fluxes were Maxwellian energy distributions; the same moderate solar activity MSIS-86 model atmosphere was used. Ionization rates for Q_0=1 erg cm^{-2} s^{-1}, E_0=1, 2, 5, and 10 keV are plotted as a function of altitude in Figure 2a. Ionization rates for Q_0=1 erg cm^{-2} s^{-1}, E_0=2 keV are plotted in Figure 2b for cases with varying initial pitch angles. Results for initial pitch angle cosines μ=0.2, 0.5, and 1.0 are compared to the standard isotropic (over the downward hemisphere) input flux. It is notable that even for an extreme case such as an electron beam aligned with the magnetic field (μ=1), there is little effect on the altitude of peak ionization rate for elec-

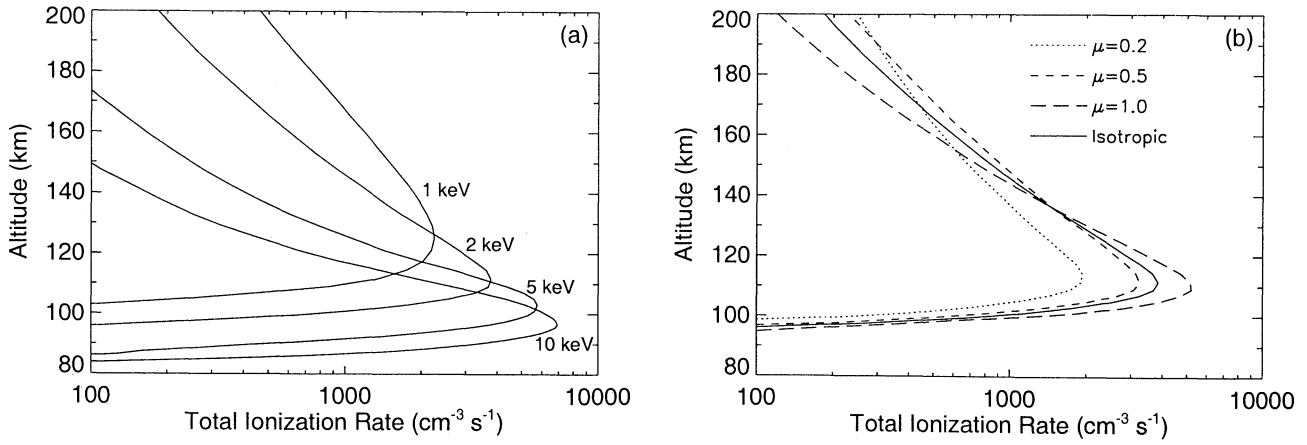

Figure 2. Ionization rate profiles calculated as a function of altitude for electron aurora. (a) Ionization rates for Q_0=1 erg cm^{-2} s^{-1}, E_0=1, 2, 5, and 10 keV. (b) Ionization rates for E_0=2 keV at initial pitch angle cosines μ=0.2, 0.5, 1.0, and isotropic (over the downward hemisphere). All input fluxes were Maxwellian energy distributions; an MSIS-86 model atmosphere with moderate solar activity, $F_{10.7}$=<$F_{10.7}$>=150, was used.

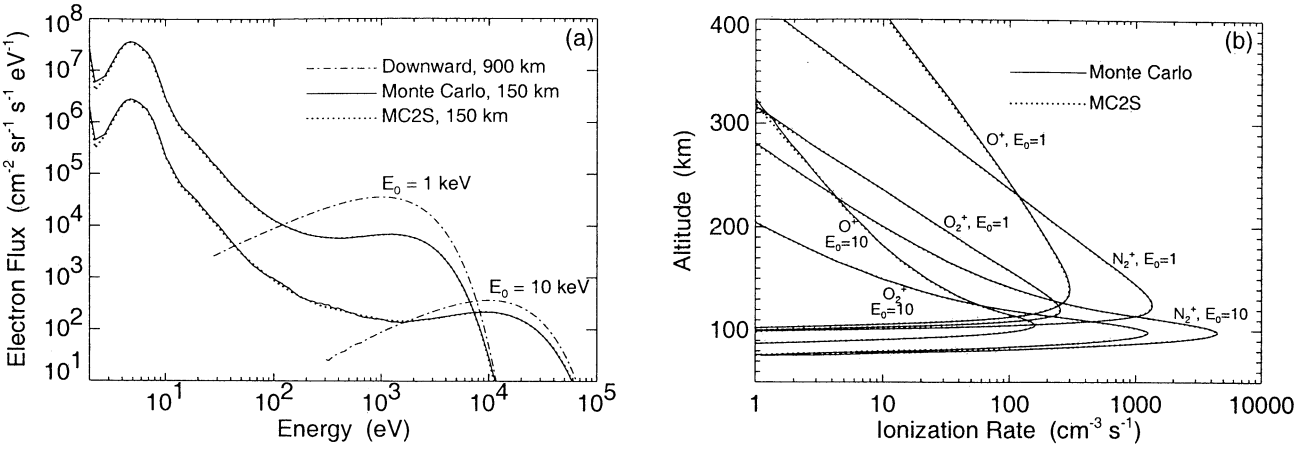

Figure 3. Comparison of the Monte Carlo model to the Monte Carlo / two-stream (MC2S) model for an isotropic Maxwellian input flux of electrons with Q_0=1 erg cm^{-2} s^{-1}, E_0=1 keV. The same model atmosphere was used as in Figures 1 and 2. (a) Input hemispherical flux at 900 km and omnidirectional flux at 150 km. (b) Ionization and selected excitation rates as a function of altitude.

trons at typical auroral energies. However, the shape of the profile can vary considerably with the initial value of μ.

Results from the Monte Carlo and MC2S models were compared for a variety of input conditions and altitudes, and negligible differences were found. Here, a comparison for isotropic Maxwellian input fluxes of electrons with E_0=1 and 10 keV, Q_0=1 erg cm^{-2} s^{-1}, are shown. The same model atmosphere was used as in Figures 1 and 2. Selected model fluxes are shown in Figure 3a, including the input hemispherical flux at 900 km and the angle-averaged omnidirectional flux at 150 km. Ionization rates produced by these runs are displayed in Figure 3b. The curves represent the total ionization rate for each species, including dissociative ionization. Ionization rates are in close agreement, within 1–3% at all but the highest altitudes, where rates are low and statistics are less robust.

3.2. Protons

Model proton and hydrogen atom fluxes are displayed as a function of altitude and energy in Figure 4. A Maxwellian proton flux, total energy flux Q_0=1 erg cm^{-2} s^{-1}, characteristic energy E_0=8 keV, isotropic over the downward hemisphere, was input at 900 km. Figure 4a shows the proton flux and Figure 4b shows the hydrogen atom flux, in both cases averaged over the downward hemisphere. The MSIS-90 [*Hedin*, 1991] model atmosphere for high solar activity conditions, $F_{10.7}$=289, $\langle F_{10.7}\rangle$=209, A_p=15, was used to facilitate comparisons to other published work.

In Figure 5, ionization rate profiles calculated as a function of altitude for proton aurora are plotted. Characteristic energies of 4, 8, 20, and 100 keV were used, as shown in Figures 5 a, b, c, d, respectively. All input fluxes were isotropic Maxwellians with Q_0=1 erg cm^{-2} s^{-1}, and the same model atmosphere as in Figure 4 was employed. Ionization rates by the primary (H^+ and H) flux and by secondary electrons are shown, and their sum, which is the total ionization rate. As the characteristic energy increases, secondary electron ionization becomes progressively more important as the secondary spectrum hardens (increases in average energy).

4. Comparison With Other Work

4.1. Electrons

Results from the Monte Carlo electron model have been compared to the two-stream calculation of auroral electron transport

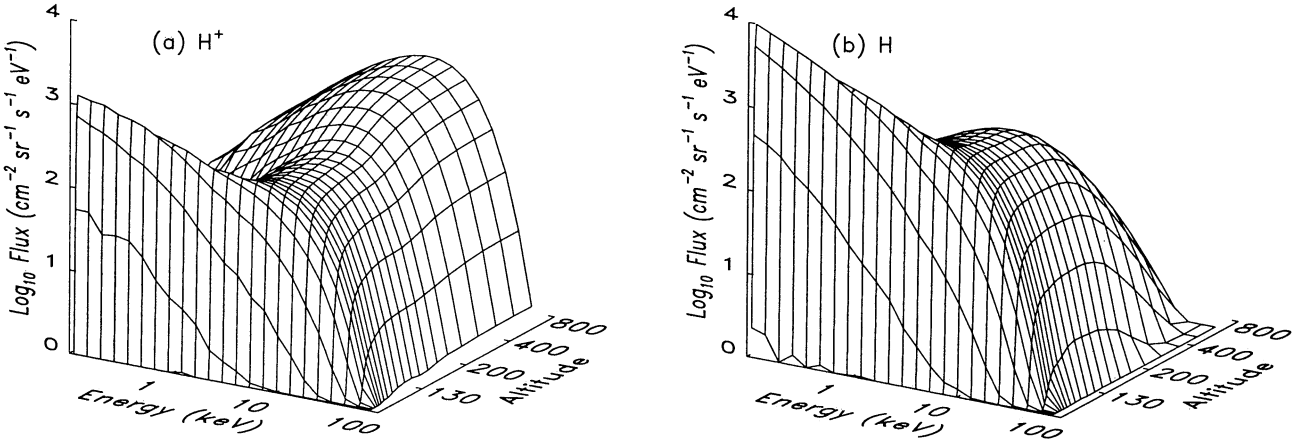

Figure 4. Model proton and hydrogen atom fluxes as a function of altitude and energy. A Maxwellian proton flux, Q_0=1 erg cm^{-2} s^{-1}, E_0=8 keV, isotropic over the downward hemisphere, was input at 900 km. (a) Proton flux averaged over the downward hemisphere. (b) Hydrogen atom flux averaged over the downward hemisphere.

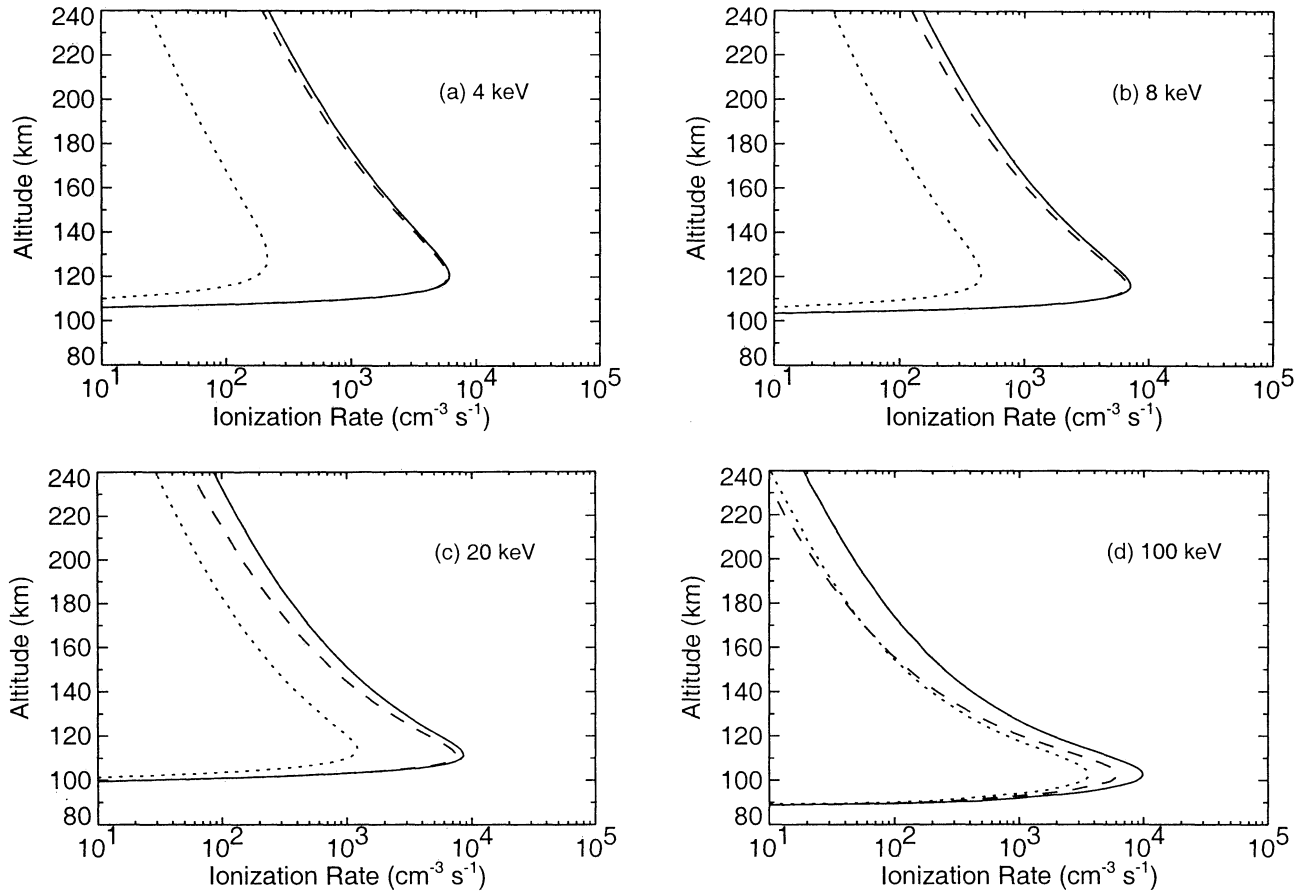

Figure 5. Ionization rate profiles calculated as a function of altitude for proton aurora: (a) E_0=4 keV, (b) E_0=8 keV, (c) E_0=20 keV, (d) E_0=100 keV. Dashed lines: primary ionization rate from protons and hydrogen atoms; dotted lines: secondary electron ionization rate; solid lines: total ionization rate. All input fluxes were isotropic Maxwellians with Q_0=1 erg cm^{-2} s^{-1}; an MSIS-90 model atmosphere with high solar activity, $F_{10.7}$=289, $<F_{10.7}>$=209, A_p=15, was used.

used by *Solomon et al.* [1988] and *Solomon* [1989], which is an extension of the photoelectron algorithm of *Banks and Nagy* [1970]. A comparison for auroral energies was shown by *Solomon* [1993], obtaining good agreement for E_0=2 keV but less satisfactory agreement at 10 keV and above, attributed to insufficient altitude grid resolution in the two-stream model. The grid resolution was increased to facilitate higher energy calculations by both models, and a comparison is shown for four orders of magnitude in E_0 in Figure 6a, using hemispherically isotropic fluxes, Q_0=1 erg cm^{-2} s^{-1}, in all cases. Here, the MC2S model

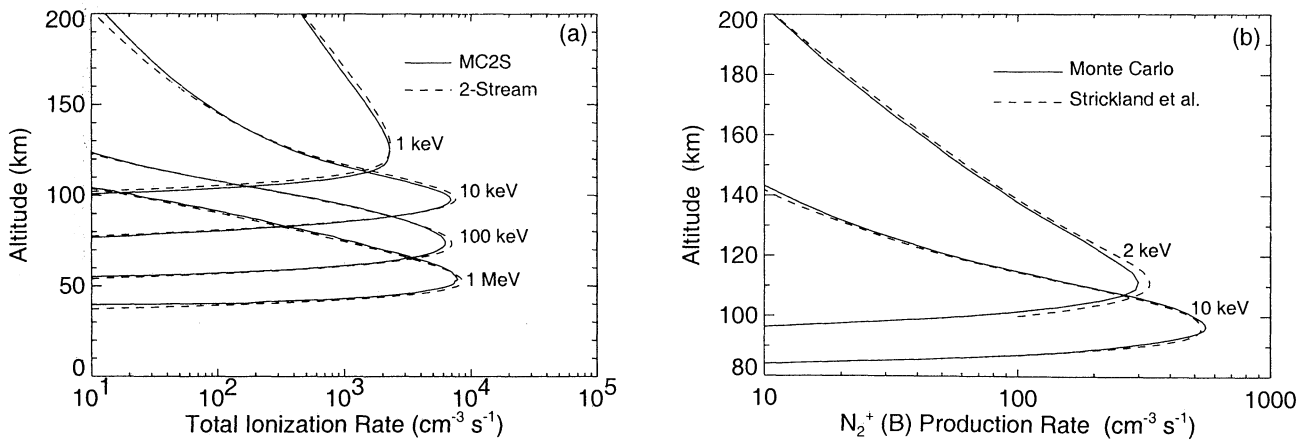

Figure 6. Comparison of ionization rates for electron aurora, calculated using different methods. (a) MC2S and two-stream models, extended to high energies. (b) Monte Carlo and multi-stream [*Strickland et al.*, 1989] models. Here the N_2^+ ($B\ ^2\Sigma_u^+$) production rate is shown instead of the total ionization rate. All fluxes were Maxwellian distributions with Q_0=1 erg cm^{-2} s^{-1} and the indicated E_0, isotropic over the downward hemisphere. The MSIS-86 $F_{10.7}$=$<F_{10.7}>$=150 atmosphere was used.

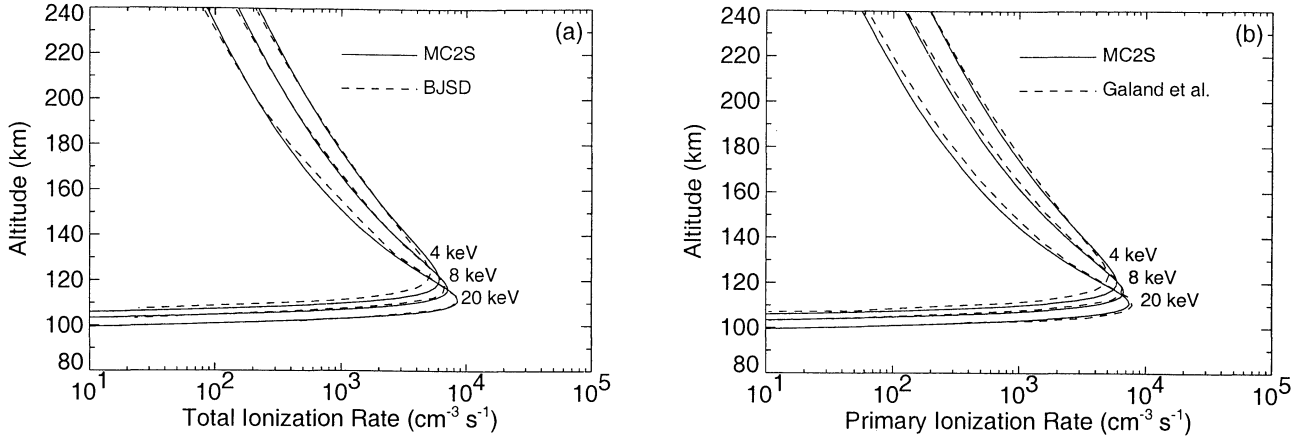

Figure 7. Comparison of ionization rates for proton aurora, calculated using different methods. (a) MC2S total ionization rates compared to the model of Basu, Jasperse, Strickland, and Daniell (BJSD) [*Basu et al.*, 1993; *Strickland et al.*, 1993]. (b) MC2S primary ionization rates compared to the model of *Galand et al.* [1997, 1998]. All fluxes were Maxwellian distributions with Q_0=1 erg cm^{-2} s^{-1} and the indicated E_0, isotropic over the downward hemisphere. The MSIS-90 atmosphere, $F_{10.7}$=289, $<F_{10.7}>$=209, A_p=15, was used.

was used instead of the full Monte Carlo to facilitate the high-energy calculations. The z_{max} predicted by the two models is in excellent agreement over all energies. This is also true for comparisons with the multi-stream equation of transfer model of *Strickland et al.* [1976, 1989, 1993], as shown in Figure 6b. Results for excitation of the $N_2^+(B)$ state were provided by D. J. Strickland (personal communication, 1992) and so are compared here instead of the total ionization rate, as it is directly proportional to the N_2 ionization rate. Isotropic Maxwellian distributions with Q_0=1 erg cm^{-2} s^{-1} were again employed for the E_0=2 keV and E_0=10 keV cases plotted here. The MSIS-86 $F_{10.7}$=$<F_{10.7}>$=150 atmosphere was used. In general, these results are in accord with the Strickland et al. model for flux distributions and ionization/excitation rates. In particular, for characteristic energies greater than ~1 keV, no significant variation is predicted in the $N_2(C)$ to $N_2^+(B)$ excitation rate ratio, and thus in the N_2 2P to N_2^+ 1N band system emission rates. This is in agreement with *Richards and Torr* [1990], *Solomon* [1993], *Strickland et al.* [1993], and *Lummerzheim and Lilensten* [1994]. The model $N_2(C)$ to $N_2^+(B)$ excitation rate ratio is 0.75 to 0.77 for E_0 > 1 keV, which translates into a ratio of 0.90 for the 2P(0,0) to 1N(0,1) (3371Å to 4278Å) vertical column brightness ratio, in good agreement with previous modeling and observations [*Solomon*, 1989].

4.2. Protons

Comparisons of ionization rates for proton aurora are shown in Figure 7. In Figure 7a, Monte Carlo model total ionization rates are compared to the model of Basu, Jasperse, Strickland, and Daniell (BJSD) [*Basu et al.*, 1993; *Strickland et al.*, 1993]. All fluxes were Maxwellian distributions with Q_0=1 erg cm^{-2} s^{-1} and E_0=4, 8, and 20 keV, isotropic over the downward hemisphere. The MSIS-90 $F_{10.7}$=289, $<F_{10.7}>$=209, A_p=15 atmosphere was used. These are the same runs as those shown in Figure 5.

Agreement is excellent at 8 keV, very good at 20 keV, and only fair at 4 keV. This is perplexing because the same cross sections and assumptions were used. However, the treatment of secondary electrons and the energy loss they cause to the H^+/H flux are not identical. The Monte Carlo model produces less primary ionization but more secondary ionization than the BJSD model, resulting in very similar peak ionization rates for the higher energies. This may indicate differences in low-energy electron excitation rate predictions. At 4 keV, primary ionization accounts for >97% of the total in both models, so this cannot explain the differences seen at and below the peak.

Monte Carlo primary ionization rates were also compared to results from the work of *Galand et al.* [1997, 1998]. Primary ionization rates were published in that work and compared to the BJSD primary ionization rates, so those calculations are used here. The model flux and neutral atmosphere parameters were the same as above. Agreement is also very good at the higher energies, although the Monte Carlo model is slightly lower. The discrepancy at 4 keV is similar to that observed in the comparison to the BJSD results above.

5. Discussion

Monte Carlo methods are often viewed as beneficial for validating or calibrating other models but not for the routine calculation of geophysical parameters. In fact, that has been the primary application of this model in the past, while the two-stream algorithm has been used for spectroscopic analysis and interaction with other modeling. But with implementation of the MC2S model, and the increasing speed of common desktop computers, run times of the order of a few minutes do not seem excessive, so the model may be put to more frequent use. For very high (many megavolt) energies the two-stream method is an effective and efficient approach. However, caution is still indicated, especially in the case of highly anisotropic pitch angle distributions, so Monte Carlo comparisons will still be of value.

Modification of this algorithm for computation of energetic proton and hydrogen atom fluxes and the accompanying generation of secondary electrons have been described in this paper. Correspondence with other methods is good. There are still significant uncertainties, though, particularly with respect to secondary electron production functions below ~5 keV and above ~100 keV primary energies. Electron aurora exhibits little or no dependence on the shape and magnitude of the secondary electron distribution on primary energy, but this is not the case for proton aurora if the conclusions of *Rudd* [1979, 1988] are correct. For

typical auroral proton fluxes < ~30 keV the secondary electron distribution generated by H^+/H ionization is softer and steeper than that for electrons, but with increasing energy the distribution becomes progressively harder and, above ~100 keV, progressively more uncertain, as discussed in section 2.3.

There is also a question concerning the importance of pitch angle redistribution in both elastic and inelastic collisions of H^+ and H with the neutral atmosphere. These processes are neglected in this work, as they were in the treatment by *Basu et al.* [1993]. *Galand et al.* [1997, 1998] included collisional pitch angle redistribution, but only for primary energies below 1 keV, and only for elastic, charge exchange, and electron stripping collisions. They used the Rutherford formula (a modified form of which is used here for electrons) with a screening parameter of 0.001, which results in predominantly forward scattering. This is in accord with measurements by *Newman et al.* [1986] which show extremely forward peaked phase functions for H on N_2 and O_2 at 1.5 and 5 keV, with ~99% of all collisions scattering less than 0.5°. Even at 0.5 keV, ~95% of collisions scatter less than 0.5°. In the absence of evidence to the contrary, the assumption that collisional pitch angle redistribution is negligible for keV protons and hydrogen atoms appears valid. This differs from the electron case, where collisional pitch angle redistribution by elastic scattering is an important process for typical auroral electron fluxes, although not for relativistic ones. Thus, unlike electron aurora, where z_{max} is relatively insensitive to initial pitch angle, proton aurora has significant dependence of z_{max} on the initial pitch angle distribution.

The influence of non-collisional pitch angle redistribution can also be significant. This occurs because of the convergence of magnetic field lines in the terrestrial exosphere and thermosphere, due to a process sometimes known as "magnetic mirroring." *Galand et al.* [1998] have shown that this can be important for protons, particularly at high altitude. Preliminary work [*Solomon*, 1999] has established a methodology for computation of electron pitch angle redistribution in the combined collisional/magnetic regime. That technique can be applied to protons as well. Another area where the Monte Carlo algorithm is adaptable to increased sophistication is in computation of the horizontal divergence or "beam spreading" of a H^+/H flux due to the particle's disengagement from the magnetic field during the time that it has neutral charge. These enhancements will be the subject of impending investigation.

Acknowledgments. This research was supported by NSF grant ATM–9203028 and NASA grant NAG5-5027 to the University of Colorado.

Janet G. Luhmann thanks Kunizo Onda and another referee for their assistance in evaluating this paper.

References

Banks, P. M., and A. F. Nagy, Concerning the influence of elastic scattering upon photoelectron transport and escape, *J. Geophys. Res.*, *75*, 1902, 1970.

Banks, P. M., C. R. Chappell, and A. F. Nagy, A new model for the interaction of auroral electrons with the thermosphere: spectral degradation, backscatter, optical emission, and ionization, *J. Geophys. Res.*, *79*, 1459, 1974.

Basu, B., J. R. Jasperse, R. M. Robinson, R. R. Vondrak, and D. S. Evans, Linear transport theory of auroral proton precipitation: A comparison with observations, *J. Geophys. Res.*, *92*, 5920, 1987.

Basu, B., J. R. Jasperse, D. J. Strickland, and R. E. Daniell Jr., Transport-theoretic model for the electron-proton-hydrogen atom aurora, 1, Theory, *J. Geophys. Res.*, *98*, 21,517, 1993.

Berger, M. J., S. M. Seltzer, and K. Maeda, Energy deposition by auroral electrons in the atmosphere, *J. Atmos. Terr. Phys.*, *32*, 1015, 1970.

Berger, M. J., S. M. Seltzer, and K. Maeda, Some new results on electron transport in the atmosphere, *J. Atmos. Terr. Phys.*, *36*, 591, 1974.

Burnett, T., and S. P. Rountree, Differential and total cross sections for electron-impact ionization of atomic oxygen, *Phys. Rev. A*, *20*, 1468, 1979.

Cicerone, R. J., and S. A. Bowhill, Photoelectron fluxes in the ionosphere generated by a Monte Carlo method, *J. Geophys. Res.*, *76*, 8299, 1971.

Crooks, J. G., and M. E. Rudd, Angular and energy distribution of cross sections for electron production by 50–300 keV proton impacts on N_2, O_2, Ne, and Ar, *Phys. Rev. A*, *3*, 1628, 1971.

Doering, J. P., and E. E. Gulcicek, Absolute differential and integral electron excitation cross sections for atomic oxygen, 8, The $^3P - {}^5S^0$ transition (1356Å) from 13.9 to 30 eV, *J. Geophys. Res.*, *94*, 2733, 1989.

Galand, M., Introduction to the special section: Proton precipitation into the atmosphere, *J. Geophys. Res.*, this issue.

Galand, M., J. Lilensten, W. Kofman, and R. B. Sidge, Proton transport model in the ionosphere, 1, Multistream approach of the transport equations, *J. Geophys. Res.*, *102*, 22,261, 1997.

Galand, M., J. Lilensten, W. Kofman, and D. Lummerzheim, Proton transport model in the ionosphere, 2, Influence of magnetic mirroring and collisions on the angular redistribution in a proton beam, *Ann. Geophys.*, *16*, 1308, 1998.

Gattinger, R. L., E. J. Llewellyn, and A. Vallance Jones, Auroral emissions and atomic oxygen densities, *Ann. Geophys.*, *14*, 687, 1996.

Green, A. E. S., and T. Sawada, Ionization cross sections and secondary electron distributions, *J. Atmos. Terr. Phys.*, *34*, 1719, 1972.

Green, A. E. S., and R. S. Stolarski, Analytic models of electron impact excitation cross sections, *J. Atmos. Terr. Phys.*, *34*, 1703, 1972.

Gulcicek, E. E., and J. P. Doering, Absolute differential and integral electron excitation cross sections for atomic oxygen, 5, Revised values for the $^3P - {}^3S^0$ (1304Å) and $^3P - {}^3D^0$ (989Å) transitions below 30 eV, *J. Geophys. Res.*, *93*, 5879, 1988.

Gulcicek, E. E., J. P. Doering, and S. O. Vaughan, Absolute differential and integral cross sections for atomic oxygen, 6, The $^3P - {}^3P$ and $^3P - {}^5P$ transitions from 13.87 to 100 eV, *J. Geophys. Res.*, *93*, 585, 1988.

Hedin, A. E., MSIS–86 thermospheric model, *J. Geophys. Res.*, *92*, 4649, 1987.

Hedin, A. E., Extension of the MSIS thermosphere model into the middle and lower atmosphere, *J. Geophys. Res.*, *96*, 1159, 1991.

Jackman, C. H., R. H. Garvey, and A. E. S. Green, Electron impact on atmospheric gases: I. Updated cross-sections, *J. Geophys. Res.*, *82*, 5081, 1977.

Kozelov, B. V., Influence of the dipolar magnetic field on transport of proton-H atom fluxes in the atmosphere, *Ann Geophys.*, *11*, 697, 1993.

Kozelov, B. V., and V. E. Ivanov, Monte-Carlo calculation of proton-hydrogen atom transport in N_2, *Planet. Space Sci.*, *40*, 1503, 1992.

Kozelov, B. V., and V. E. Ivanov, Effective energy loss per electron-ion pair in proton aurora, *Ann Geophys.*, *12*, 1071, 1994.

Link, R., Dayside magnetospheric cleft auroral processes, Ph.D. thesis, York Univ., Toronto, Ont, Canada, 1982.

Lummerzheim, D., and J. Lilensten, Electron transport and energy degradation in the ionosphere: Evaluation of the numerical solution, comparison with laboratory experiments and auroral observations, *Ann. Geophys.*, *12*, 1039, 1994.

Lummerzheim, D., M. H. Rees, and H. R. Anderson, Angular dependent transport of auroral electrons in the upper atmosphere, *Planet. Space Sci.*, *37*, 109, 1989.

Meier, R. R., and J.-S. Lee, A Monte Carlo study of frequency redistribution in an externally excited medium, *Astrophys. J.*, *219*, 262, 1978.

Newman, J. H., Y. S. Chen, K. A. Smith, and F. R. Stebbings, Differential cross sections for scattering of 0.5-, 1.5-, and 5.0 keV hydrogen atoms by He, H_2, N_2, and O_2, *J. Geophys. Res.*, *91*, 8947, 1986.

Onda, K., M. Hayashi, and K. Takayanagi, Monte Carlo calculation of ionization and excitation rates in electron aurora, *Rep. 645, Inst. of Space and Astron. Sci.*, Kanagawa, Japan, 1992.

Opal, C. B., W. K. Peterson, and E. C. Beaty, Measurements of secondary-electron spectra produced by electron impact ionization of a number of simple gases, *J. Chem. Phys.*, *55*, 4100, 1971.

Porter, H. S., and A. E. S. Green, Comparison of Monte Carlo and continuous slowing-down approximation treatments of 1-keV proton energy deposition in N_2, *J. Appl. Phys.*, *46*, 5030, 1975.

Porter, H. S., and F. W. Jump, Analytic total and angular elastic electron impact cross sections for planetary atmospheres, *Tech. Rep. CSC/TM-6017*, Goddard Space Flight Cent., Greenbelt, Md., 1978.

Porter, H. S., C. H. Jackman, and A. E. S. Green, Efficiencies for production of atomic nitrogen and oxygen by relativistic proton impact in air, *J. Chem. Phys.*, *65*, 154, 1976.

Porter, H. S., F. Varosi, and H. G. Mayr, Iterative solution of the multistream electron transport equation, 1, Comparison with laboratory beam injection experiments, *J. Geophys. Res.*, *92*, 5933, 1987.

Rees, M. H., and D. Lummerzheim, Characteristics of auroral electron precipitation derived from optical spectroscopy, *J. Geophys. Res.*, *94*, 6799, 1989.

Richards, P. G., and D. G. Torr, Auroral modeling of the 3371 Å emission rate: dependence on characteristic electron energy, *J. Geophys. Res.*, *95*, 10337, 1990.

Rieke, F. F., and W. Prepejchal, Ionization cross sections of gaseous atoms and molecules for high-energy electrons and positrons, *Phys. Rev. A*, *6*, 1507, 1972.

Rudd, M. E., Energy and angular distributions of secondary electrons from 5–100 keV proton collisions with hydrogen and nitrogen molecules, *Phys. Rev. A*, *20*, 787, 1979.

Rudd, M. E., Differential cross sections for secondary electrons production by proton impact, *Phys. Rev. A*, *38*, 6129, 1988.

Saksena, V., M. S. Kushwaha, and S. P. Khare, Electron impact ionisation of molecules at high energies, *Int. J. Mass Spectrom. Ion Processes.*, *171*, L1, 1997.

Solomon, S. C., Auroral excitation of the N_2 2P(0,0) and VK(0,9) bands, *J. Geophys. Res.*, *94*, 17215, 1989.

Solomon, S. C., Auroral electron transport using the Monte Carlo method, *Geophys. Res. Lett.*, *20*, 185, 1993.

Solomon, S. C., Where is the loss cone?, paper presented at Chapman Conference on Atmospheric Science Across the Stratopause, AGU, Annapolis, Md., 1999.

Solomon, S. C., and V. J. Abreu, The 630 nm dayglow, *J. Geophys. Res.*, *94*, 6817, 1989.

Solomon, S. C., P. B. Hays, and V. J. Abreu, The auroral 6300 Å emission: Observations and modeling, *J. Geophys. Res.*, *93*, 9867, 1988.

Strickland, D. J., D. L. Book, T. P. Coffey, and J. A. Fedder, Transport equation techniques for the deposition of auroral electrons, *J. Geophys. Res.*, *81*, 2755, 1976.

Strickland, D. J., R. R. Meier, J. H. Hecht, and A. B. Christensen, Deducing composition and incident electron spectra from ground based auroral optical measurements: Theory and model results, *J. Geophys. Res.*, *94*, 13,527, 1989.

Strickland, D. J., R. E. Daniell Jr., B. Basu, and J. R. Jasperse, Transport-theoretic model for the electron-proton-hydrogen atom aurora, 2, Model results, *J. Geophys. Res.*, *98*, 21,533, 1993.

Swartz, W. E., J. S. Nisbet, and A. E. S. Green, Analytical expression for the energy transfer rate from photoelectrons to thermal electrons, *J. Geophys. Res.*, *76*, 8425, 1971.

Synnes, S. A., F. Søraas, and J. P. Hansen, Monte-Carlo simulations of proton aurora, *J. Atmos. Sol. Terr. Phys.*, *60*, 1695, 1998.

Toburen, L. H., Distributions in energy and angle of electrons ejected from molecular nitrogen by 0.3- to 1.7-MeV protons, *Phys. Rev. A.*, *3*, 216, 1971.

S. C. Solomon, Laboratory for Atmospheric and Space Physics, 1234 Innovation Dr., University of Colorado, Boulder, CO 80309-0590 (solomon@lasp.colorado.edu)

(Received February 22, 2000; revised June 18, 2000;
accepted July 7, 2000.)